



Hydrogen generation from the hydrolytic dehydrogenation of ammonia borane using electrolessly deposited cobalt–phosphorus as reusable and cost-effective catalyst

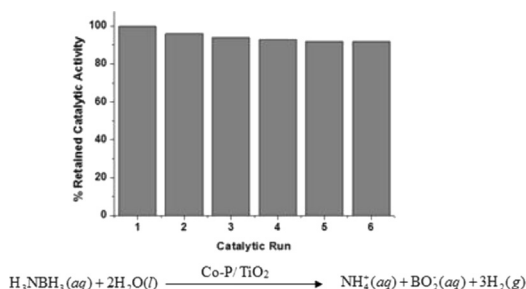
Murat Rakap*

Department of Chemistry, Yüzüncü Yıl University, 65080 Van, Turkey

HIGHLIGHTS

- Co–P/TiO₂ is efficient, reusable, and low-cost catalyst for hydrolytic dehydrogenation of AB.
- The catalyst is reusable with minimal loss of activity for several cycles.
- Arrhenius activation energy is found to be $48.1 \pm 2 \text{ kJ mol}^{-1}$.

GRAPHICAL ABSTRACT



ARTICLE INFO

Article history:

Received 24 March 2014

Received in revised form

17 April 2014

Accepted 23 April 2014

Available online 2 May 2014

Keywords:

Electroless deposition

Cobalt

Ammonia borane

Hydrolytic dehydrogenation

Hydrogen

ABSTRACT

The development of catalytically active, low-cost, and reusable catalysts is very vital for on-demand hydrogen generation systems for practical onboard applications. Titanium dioxide supported-cobalt–phosphorus (Co–P/TiO₂) catalyst prepared by electroless deposition has been shown to effectively promote the release of hydrogen from the hydrolytic dehydrogenation of ammonia borane. The catalyst is very stable to be isolated as solid material and characterized by XRD, SEM-EDX, and XPS. It is redispersible and reusable as an active catalyst in the hydrolytic dehydrogenation of AB. The activation energy (E_a) for the hydrolytic dehydrogenation of ammonia borane catalyzed by Co–P/TiO₂ catalyst is $48.1 \pm 2 \text{ kJ mol}^{-1}$. Maximum hydrogen generation rate in the hydrolytic dehydrogenation of ammonia borane catalyzed by Co–P/TiO₂ catalyst is $2002 \text{ mL H}_2 \text{ min}^{-1} (\text{g catalyst})^{-1}$.

© 2014 Elsevier B.V. All rights reserved.

1. Introduction

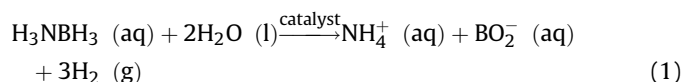
Hydrogen has become one of the most promising future energy carriers in recent years due to the concerns over the depletion of fossil fuels supplies, environmental pollution and global warming which is attributable to the greenhouse effect caused by a steep

increase in carbon dioxide and other gases [1,2]. However, the lack of effective and safe hydrogen-storage materials is the most important challenge toward hydrogen-powered society as a long-term solution for a secure energy future [3]. Recently, ammonia borane (H₃NBH₃, AB) has been considered to be a promising candidate as an efficient hydrogen-storage material to meet the 2010 targets (6 wt % and 45 g L^{-1}) and potentially meet the 2015 targets (9 wt % and 81 g L^{-1}) set by the U.S. Department of Energy (DOE) [4,5] due to its high hydrogen content (19.6 wt % H₂) and low molecular weight (30.7 g mol^{-1}) [6,7]. It is highly soluble in water

* Tel.: +90 432 225 17 01; fax: +90 432 486 54 13.

E-mail addresses: mrtrakap@gmail.com, muratrakap@gmail.com.

and its solution is stable at room temperature. However, it releases hydrogen gas upon hydrolytic dehydrogenation at room temperature in the presence of suitable catalysts (Eq. (1)) [8].



So far, various catalyst systems consisting of noble and non-noble metals have been tested as catalysts for hydrogen generation from the hydrolysis of AB. Generally, the catalysts composed of noble metals showed higher catalytic activities. However, development of low-cost and efficient catalysts is desired for practical uses. Recent advances in catalyst preparation technologies have led to significant improvements in the catalytic activity of transition metal catalysts, even to a level comparable to that of the noble metal catalysts [9]. Particularly, supported non-noble transition metals can be employed as active catalysts in practical applications owing to their easy separation from the solution and reusability [10]. Some of the non-noble catalysts used for the hydrolysis of AB are hollow titania–nickel composite [11], graphene supported cobalt(0) nanoparticles [12], amorphous Co–B catalyst [13], mesoporous silica supported Co–B [14], Co–B, Ni–B, Cu–B [15], hollow nickel–silica composite [16], Co–B [17], amorphous nickel catalyst [18], polymer-stabilized iron(0) nanoclusters [19], hydroxyapatite-supported cobalt(0) nanoclusters [20], Co/IR-120 [21], Co–P–B/Ni foam [22], Co–B/C [23], silica embedded Co(0) nanoclusters [24], Co₃O₄ [25], Co–W–B–P/Ni [26], Co–SiO₂ nanosphere [27], intrazeolite cobalt(0) nanoclusters [28], nanoparticle-assembled Co–B [29], Co nanoparticles [30], Co–Mo–B/Ni [10], Fe–Ni alloy [31], PVP-stabilized nickel [8], and Co–M–B–P [32].

Herein, the preparation and characterization of electrolessly deposited Co–P catalysts on TiO₂ and their use as catalyst in the hydrolytic dehydrogenation of ammonia borane is reported. Electroless deposition, an autocatalytic redox reaction process which provides a uniform and dense coating on all surface area of the plating support regardless of the configuration or geometry of the support [33], is the most popular and efficient method to prepare supported non-noble transition metal catalysts [34]. Indeed, a study [35] has shown that Co–Ni–P catalyst prepared by electroless deposition method on the surface TiO₂ can be used as active catalyst in the hydrolytic dehydrogenation of AB. In the light of the results of kinetic studies (depending on the catalyst amount, substrate concentration, and temperature) and the reusability experiment, Co–P/TiO₂ catalysts can be regarded as efficient, low-cost, and reusable catalysts in the hydrolytic dehydrogenation of AB to produce hydrogen. The main advantages of the catalyst are its low-cost and high reusability.

2. Experimental section

2.1. Materials

Cobalt sulfate heptahydrate, sodium hypophosphite monohydrate, EDTA, gluconic acid, boric acid, ammonium hydroxide, sodium potassium tartrate, ammonia–borane complex (97%), palladium acetate, butvar (B98), and titanium dioxide (Degussa P-25) were purchased from Aldrich. All chemicals were used as received. Deionized water was distilled by water purification system.

2.2. Preparation of the Co–P catalyst

The Co–P catalyst was prepared and supported on Pd–TiO₂ by using electroless deposition method. Cobalt sulfate heptahydrate

Table 1

Bath composition and the operating conditions employed for preparing electrolessly deposited Co–P catalyst on TiO₂.

Catalyst	Co–P
<i>Bath composition</i>	
Cobalt sulfate heptahydrate (mM)	53.08
Sodium hypophosphite monohydrate (M)	0.094
Gluconic acid (M)	0.023
EDTA (M)	0.013
Sodium potassium tartrate (M)	0.035
Boric acid (M)	0.162
<i>Operating conditions</i>	
pH	10.5
Temperature (°C)	75 ± 2
Time (min)	45

was used as the source of cobalt. Sodium hypophosphite was used as the reducing agent, which also forms the source of phosphorus in the deposit. EDTA was used as the complexing agent to control the rate of release of free metal ion for the reduction reaction. In addition to other constituents, ammonium hydroxide was added to adjust the pH of the bath solution. During plating, the bath was maintained at a temperature of 75 ± 2 °C by a constant temperature bath. The bath composition and operating conditions employed for the preparation of electroless Co–P alloy deposits are given in Table 1.

Since the electroless deposition of Co–P alloy requires a catalytically active surface, titanium dioxide surface has to be activated. For this purpose, 1 g of titanium dioxide was mixed with 12 g of catalyst ink solution by a method described in detail elsewhere [36,37]. The polymer-stabilized palladium catalyst ink solution was prepared by dissolving a specified amount (0.2–0.5 g) of analytical reagent grade palladium acetate trimer [CH₃(CO₂)₂Pd] (47.05% Pd) from Aldrich–Sigma Co, in 2.0 mL NH₄OH. The palladium mixture was then added with stirring for several hours into a base solution of poly vinyl butyral (PVB) in methanol. The alcoholic-polymer base solution contained 2.0 g poly (vinyl) butyral (Solutia Inc.'s Butvar B-98) in a known volume (100–200 mL) of methanol. The amount of PVB dissolved in alcohol can be used to adjust the catalyst ink viscosity. After a thorough mixing, the as-prepared catalyst solution can be preserved for years without loss in its activity.

The titanium dioxide-catalyst ink mixture was stirred to prepare Pd-activated TiO₂ for 2 h at room temperature, and kept at 270 °C for 48 h and then 350 °C for 6 h. To initiate the electroless

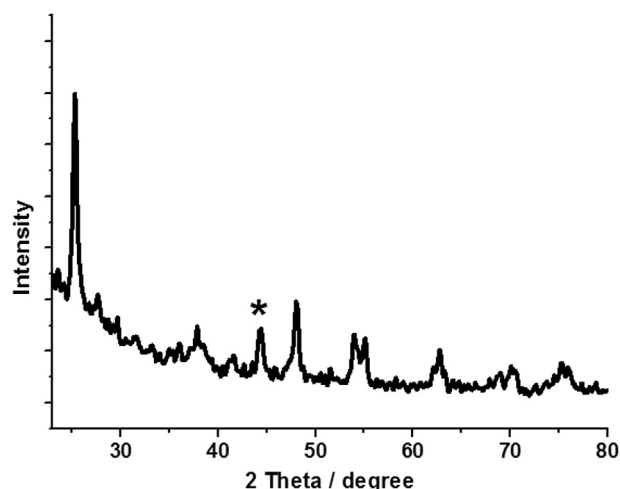


Fig. 1. XRD patterns of the Co–P/TiO₂ catalyst prepared by electroless deposition.

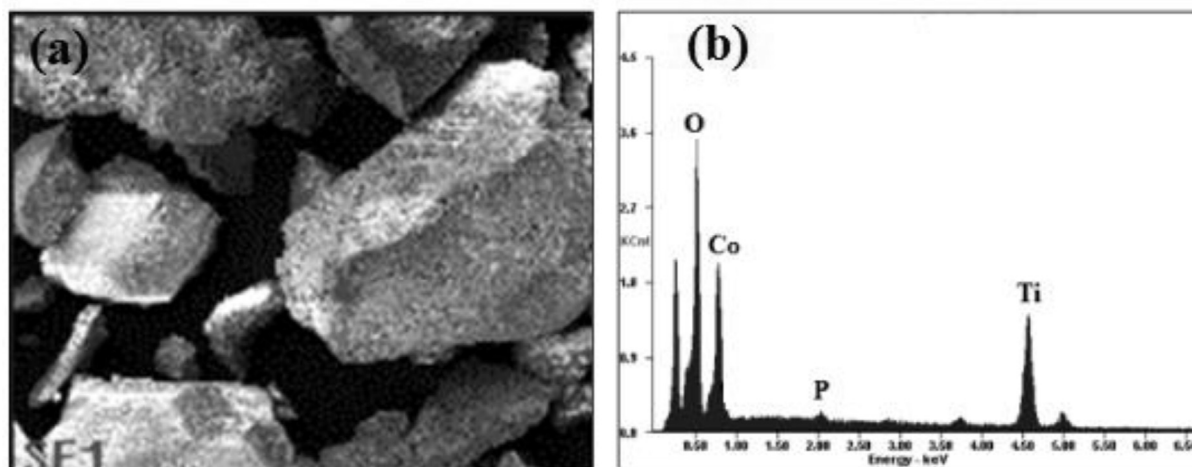


Fig. 2. The SEM micrograph (a) and the EDX spectrum (b) of the Co–P/TiO₂ catalyst.

deposition process, 0.2 g of activated titanium dioxide was added into the 25 mL of electroless plating bath solution. The electroless Co–P particle deposition was conducted for 45 min. The reaction was then terminated by rapid cooling of plating bath with the addition of cold water. These Co–P/TiO₂ particles were easily collected by centrifugation, and then washed with deionized water and methanol before drying in the oven at 50 °C.

2.3. Catalytic evaluation of Co–P catalyst in the hydrolytic dehydrogenation of AB

The catalytic activity of electrolessly deposited Co–P/TiO₂ catalyst in the hydrolytic dehydrogenation of AB was determined

by measuring the rate of hydrogen generation. In all experiments, the reaction flask (30 mL) was placed in a thermostat that was equipped with a water circulating system, wherein the temperature was kept constant at 25 ± 0.5 °C. Then, a graduated burette (50 mL) filled with water was connected to reaction flask to measure the volume of the hydrogen gas to be evolved from the reaction. Next, 31.8 mg (1.0 mmol) AB was dissolved in 20 mL water. This solution was transferred with a glass pipette into the reaction flask thermostated at 25 ± 0.5 °C. Then, certain amount of Co–P/TiO₂ (25, 50, 75, and 100 mg, respectively) catalyst was added into the reaction flask. The reaction was started by closing the flask and the volume of hydrogen gas evolved was measured by recording the displacement of water level from the graduated burette as the reaction

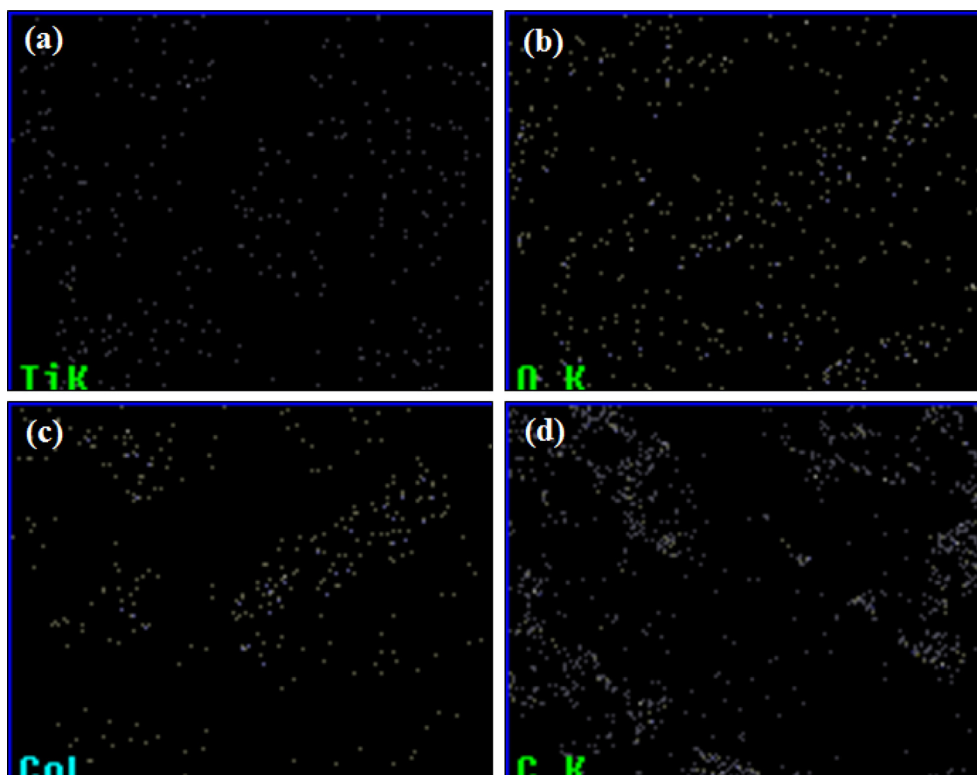


Fig. 3. The mapped SEM micrographs of the elements in the catalyst; (a) Ti, (b) O, (c) Co, and (d) C.

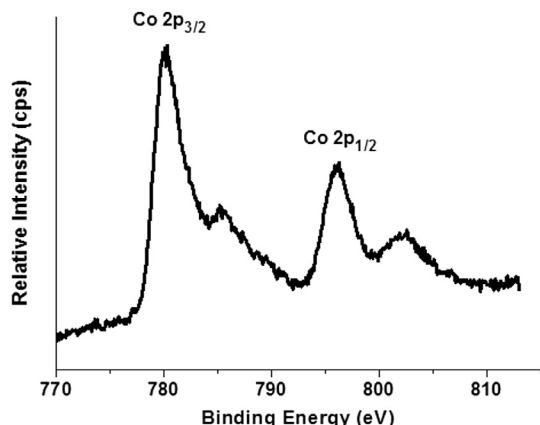


Fig. 4. High resolution X-ray photoelectron spectrum of Co–P/TiO₂ catalyst showing cobalt 2p regions.

progressed. In addition to the volumetric measurement of the hydrogen evolution, the conversion of AB ($\delta = -23.9$ ppm) to metaborate ($\delta = 9.0$ ppm) was also checked by ¹¹B NMR spectroscopy.

2.4. The effect of stirring speed on hydrogen generation rate

The same experiment described in Section 2.3 for the hydrogen generation from the hydrolytic dehydrogenation of AB was performed at 25 ± 0.5 °C by varying the stirring speed (0, 200, 400, 600, 800, 1000, and 1200 rpm) to check how hydrogen generation rate was affected by stirring speed in the hydrolytic dehydrogenation of AB.

2.5. Kinetic study of the hydrolytic dehydrogenation of AB catalyzed by Co–P catalyst

In order to establish the rate law for hydrolytic dehydrogenation of AB using Co–P/TiO₂ as catalyst, two different sets of experiments were performed in the same way described in Section 2.3. In the first set of experiments, the hydrolytic dehydrogenation reaction was carried out starting with different initial amount of catalyst (25, 50, 75, and 100 mg) and keeping the initial amount of AB constant (31.8 mg, 50 mM). The second set of experiments was carried out by keeping the initial amount of catalyst constant

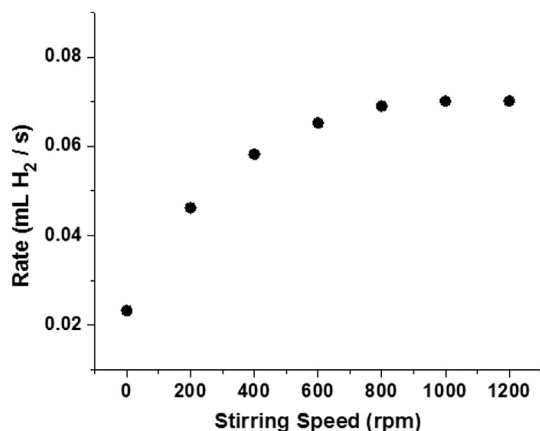


Fig. 5. Plot of hydrogen generation rate versus the stirring speed for the hydrolytic dehydrogenation of H₃NBH₃ (50 mM) catalyzed by Co–P (25 mg) catalyst at 25.0 ± 0.5 °C.

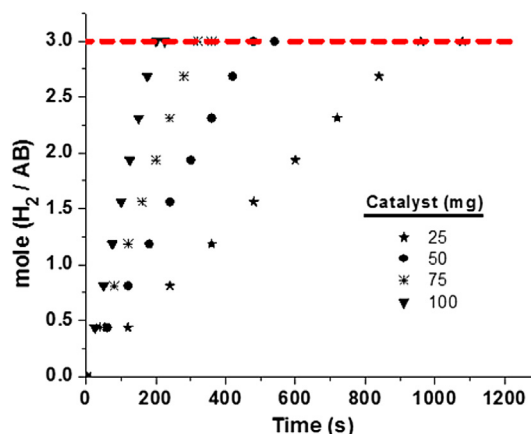


Fig. 6. Plot of mole H₂/mole H₃NBH₃ versus time (s) for the hydrolytic dehydrogenation of H₃NBH₃ (50 mM) catalyzed by Co–P catalyst with different catalyst amounts (25, 50, 75, 100 mg) at 25.0 ± 0.5 °C.

(25 mg) and varying the concentration of AB (50, 100, and 150 mM, respectively). Finally, the hydrolytic dehydrogenation of AB was carried out by keeping the amounts of Co–P/TiO₂ catalyst (25 mg) and AB (50 mM) at temperatures of 25, 35, 45, and 55 °C in order to obtain the activation energy (E_a) for this hydrolysis reaction.

2.6. Reusability of Co–P catalyst in the hydrolytic dehydrogenation of AB

After the hydrolytic dehydrogenation reaction of AB was completed, the catalyst was filtered, washed with deionized water and methanol, and dried. Then, another equivalent of aqueous AB (50 mM) solution was added to the reaction flask which contained the catalyst. The volume of the released hydrogen gas was then monitored by the gas burette. Such reusability experiments were repeated for 6 times under ambient atmosphere.

2.7. Catalyst characterization

Powder X-ray diffraction (XRD) patterns were recorded with a Rigaku X-ray Diffractometer using Cu K α radiation (30 kV, 15 mA) at room temperature. Scanning was performed between 2θ degrees of 20–80°. The measurements were made with 0.01 and 0.05° steps and 1°/min rate. The divergence slit was variable and scattering and

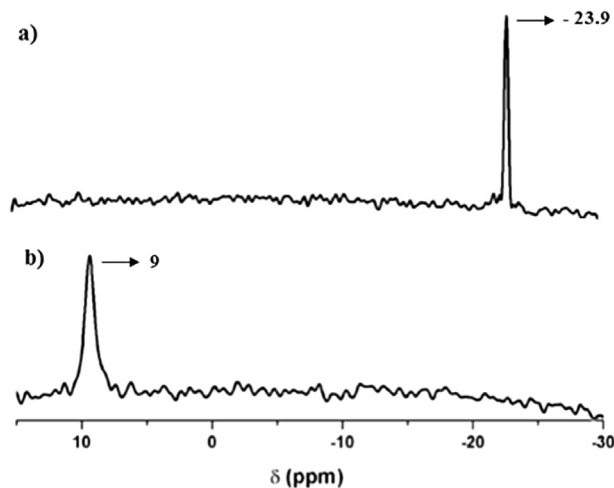


Fig. 7. ¹¹B NMR spectrum before (a) and after (b) the hydrolysis of AB.

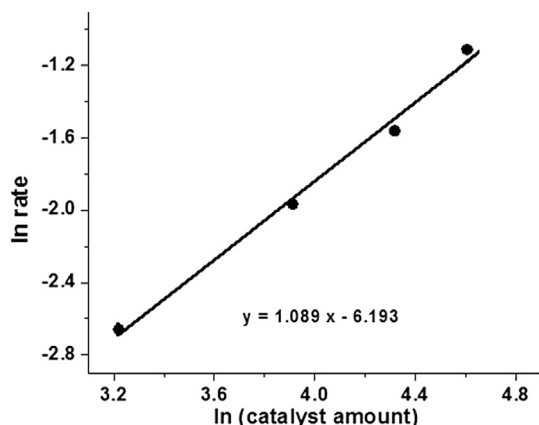


Fig. 8. Plot of hydrogen generation rate versus catalyst amount (both in logarithmic scale) for the hydrolytic dehydrogenation of H_3NBH_3 (50 mM) catalyzed by Co-P catalyst with different amount of catalyst (25, 50, 75, 100 mg) at 25.0 ± 0.5 °C.

receiving slit were 4.2° and 0.3 mm, respectively. Scanning Electron Microscopy (SEM) analysis was carried out with a Zeiss 1540 ESB scanning electron microscope operating at an accelerating voltage of 10 kV, equipped with an energy dispersive X-ray (EDX) analysis unit. X-ray photoelectron spectrum (XPS) was taken by using SPECS spectrometer equipped with a hemispherical analyzer and using monochromatic Mg-K α radiation (1250 eV, the X-ray tube working at 15 kV and 350 W). ^{11}B NMR spectra were recorded on a Bruker Avance DPX 400 with an operating frequency of 128.15 MHz for ^{11}B .

3. Results and discussion

3.1. Characterization of the catalyst

Fig. 1 shows the XRD patterns of the Co-P catalyst that electrolessly deposited on TiO_2 . This XRD patterns mainly show the support material (Degussa P-25 TiO_2 , with 80% anatase and 20% rutile composition) diffraction peaks between $2\theta = 20^\circ$ – 80° except for the sharp peak located at $2\theta = 44.5^\circ$ that indicates the (002) plane of the hexagonal close packed Co phase [38]. The anatase phase diffraction peaks are evident at the following 2θ values: 25.2° , 38° , 48.2° , 55° , and 62.5° . Similarly, the rutile phase diffraction peaks at 27.5° , 36° , 54° , and 69° are also evident.

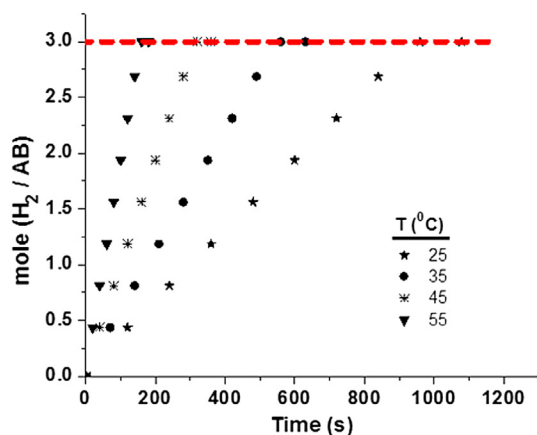


Fig. 9. Plot of mole H_2 /mole H_3NBH_3 versus time (s) for the hydrolytic dehydrogenation of H_3NBH_3 (50 mM) catalyzed by Co-P catalyst (25 mg) in the temperature range of 25 – 55 ± 0.5 °C.

Table 2

Activities in terms of maximum hydrogen generation (Max HG rate) rate values of various non-noble catalyst systems tested in hydrogen generation from the hydrolysis of AB.

Catalyst	Max HG rate (mL H_2 g catalyst $^{-1}$ min $^{-1}$)	Reference
Amorphous Co-B	5447.8	[13]
Co-B/mesoporous silica	1900	[14]
$\text{Co}_{0.75}\text{B}_{0.25}$	7607	[15]
$\text{Cu}_{0.75}\text{B}_{0.25}$	1178	[15]
$\text{Ni}_{0.75}\text{B}_{0.25}$	3869	[15]
Co-B	9157.2	[17]
Amorphous nickel	827	[18]
Co(0)/hydroxyapatite	2200	[20]
Co-P-B	2000	[22]
Co-B/C	13500	[23]
Co-W-B-P/Ni	4000	[26]
Co-B/nanoparticle	8200	[29]
Co nanoparticles	1116	[30]
Co-P/TiO$_2$	2002	[This study]
Co/mesoporous silica	258	[44]
CoCu/Ni	25	[45]
Co-Ni-P/Pd-TiO $_2$	170	[46]

The morphology and the chemical composition of the Co-P catalyst were studied by SEM and EDX, as shown in Fig. 2a and b, respectively. From EDX analysis, it was found that the only element in the catalyst apart from titanium and oxygen is cobalt, indicating the insertion of cobalt on the support. The EDX micrograph also shows the average composition (Co:P = 98.6:1.4 wt.%) taken at multiple points on the sample. Additionally, the mapped SEM micrographs of the elements (Ti, O, Co) in the catalyst are shown in Fig. 3 along with the carbon from SEM mount.

X-ray photoelectron spectra (XPS) of the Co-P catalyst given in Fig. 4 shows two prominent bands at 780 and 796.3 eV, readily attributable to Co(0) $2p_{3/2}$ and Co(0) $2p_{1/2}$, respectively [39]. Compared to the values of bulk cobalt [39] (778.5 and 794.7 eV), the Co $2p_{3/2}$ and Co $2p_{1/2}$ peaks of Co-P catalyst are shifted to higher binding energies by 1.5 and 1.6 eV, respectively. This shift might be attributed to the matrix effect of the support material or to the size effect [40]. XPS spectrum also shows two additional bands observed at slightly higher energies, which can be attributed to higher oxidation states of cobalt, presumably formed by oxidation during the XPS sample preparation, since cobalt is sensitive to oxygen. These additional weak bands can be attributed to the different cobalt(II) species, since the oxidation product may exist in different forms depending on the ligand (hydroxide, oxide, or nitrogen donor) [41].

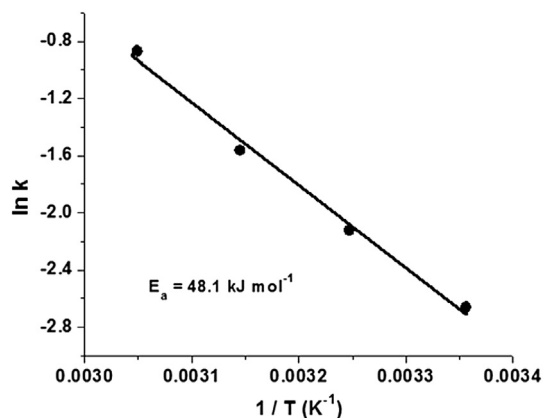


Fig. 10. Arrhenius plot for the hydrolytic dehydrogenation of H_3NBH_3 (50 mM) catalyzed by Co-P catalyst (25 mg) at 25 ± 0.5 °C.

Table 3

The apparent Arrhenius activation energy values ($E_{a,app}$, kJ mol⁻¹) for various non-noble catalyst systems tested in hydrogen generation from the hydrolysis of AB.

Catalyst	Activation energy (kJ mol ⁻¹)	Reference
Co–Mo–B/Ni	44.3	[10]
Co(0)/graphene	32.75	[12]
Co _{0.75} B _{0.25}	40.85	[15]
Cu _{0.75} B _{0.25}	48.74	[15]
Ni _{0.75} B _{0.25}	43.19	[15]
Co–B	47.5	[17]
Co(0)/hydroxyapatite	50	[20]
Co–B/C	29	[23]
Co–W–B–P/Ni	29	[26]
Co(0)/zeolite Y	56	[28]
Co–B/nanoparticle	34	[29]
Co–Ni–P/Pd–TiO ₂	54.7	[46]
Co/γ-Al ₂ O ₃	62	[47]
p(AMPS)–Co	47.7	[48]
p(AMPS)–Cu	48.8	[48]
p(AMPS)–Ni	52.8	[48]
Co–P/TiO₂	48.1	[This study]
Co(0)–MOF	35.5	[49]

3.2. The effect of stirring speed on hydrogen generation rate

The effect of stirring speed on the hydrogen generation rate in the hydrolytic dehydrogenation of AB was investigated by performing the catalytic reaction at various stirring speeds and the results are graphically presented in Fig. 5. It is seen that the hydrogen generation rate is independent of the stirring speed when it is higher than 800 rpm. This indicates that the system is in a non-mass transfer limitation regime since the present kinetic study was performed at the stirring speed of 1000 rpm.

3.3. Catalytic evaluation of Co–P in the hydrolytic dehydrogenation of AB

The kinetics of the hydrolytic dehydrogenation of AB catalyzed by Co–P/TiO₂ was studied by varying the amount of catalyst, substrate concentration and temperature. Fig. 6 shows the plots of the stoichiometric mole ratio of evolved H₂ to H₃NBH₃ versus time during the hydrolytic dehydrogenation of 50 mM AB in the presence of the different amounts of Co–P/TiO₂ at 25.0 ± 0.5 °C. The

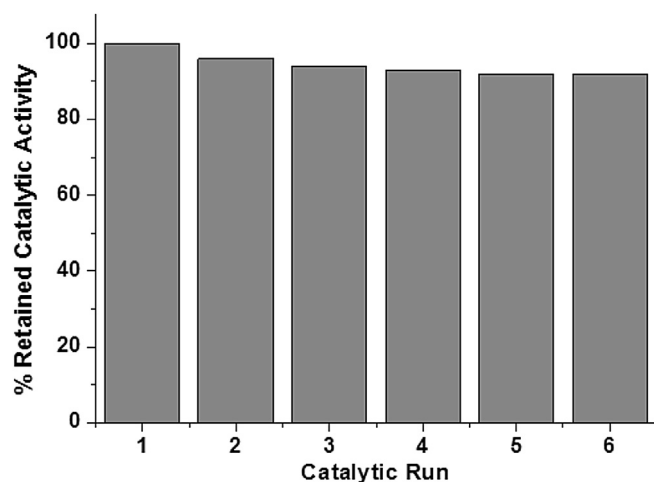


Fig. 11. % Retained catalytic activity versus number of subsequent catalytic runs for Co–P (25 mg) catalyzed hydrolytic dehydrogenation of H₃NBH₃ (50 mM) at 25 ± 0.5 °C.

linear hydrogen generation starts immediately without an induction period and continues until the complete hydrolysis of AB. The quantity of NH₃ liberated during the hydrolysis of AB has been found to be negligible when the catalyst and substrate concentrations are lower than 0.06 mol % and 6 wt %, respectively [42]. As expected, the control tests using copper(II) sulfate trap with acid-base indicators resulted in no NH₃ evolution in detectable amount in the experiments conducted in this study. Additionally, conversion of AB ($\delta = -23.9$ ppm) to metaborate ($\delta = 9$ ppm) was also checked by ¹¹B NMR spectroscopy and related spectra are given in Fig. 7.

The rates of hydrogen generation were determined from the linear portions of the plots in Fig. 6 and used to obtain the plots of the hydrogen generation rates versus initial catalyst amounts, both in logarithmic scale, as depicted in Fig. 8. The slope of the plot is 1.089, indicating that the hydrolytic dehydrogenation of AB catalyzed by Co–P/TiO₂ is first order with respect to the catalyst amount. The effect of AB substrate concentration on the hydrogen generation rate was also studied by carrying out a series of experiments starting with varying initial concentration of AB while keeping the catalyst amount constant at 25 mg. The hydrogen generation from the hydrolytic dehydrogenation of AB was found to be practically independent of AB concentration. Consequently, the rate law for the hydrolytic dehydrogenation of AB catalyzed by Co–P/TiO₂ catalyst can be given as in Eq. (2).

$$\frac{-3d[\text{NH}_3\text{BH}_3]}{dt} = \frac{d[\text{H}_2]}{dt} = k[\text{Co–P}] \quad (2)$$

Finally, Co–P/TiO₂ catalyzed hydrolytic dehydrogenation of AB was carried out at various temperatures in the range of 25–55 ± 0.5 °C, starting with a constant initial concentration of substrate (50 mM H₃NBH₃) and a constant initial amount of Co–P/TiO₂ catalyst (25 mg) and the results were plotted as in Fig. 9. Maximum hydrogen generation rate in the hydrolytic dehydrogenation of AB catalyzed by Co–P/TiO₂ catalyst is 2002 mL H₂ min⁻¹ (g catalyst)⁻¹ at 25 ± 0.5 °C. Maximum hydrogen generation rate values of some non-noble catalyst systems are given in Table 2 for comparison. Maximum hydrogen generation value of Co–P/TiO₂ catalyst appears to be quite remarkable for the hydrolysis of AB.

The values of rate constants at different temperatures for Co–P/TiO₂ catalyzed hydrolytic dehydrogenation of AB were measured from the linear portions of the plots given in Fig. 9 and used for the calculation of activation energy from the Arrhenius plot shown in Fig. 10. The Arrhenius activation energy was calculated to be 48.1 ± 2 kJ mol⁻¹ for hydrolytic dehydrogenation of AB catalyzed by Co–P/TiO₂ catalyst. Arrhenius activation values of some non-noble catalysts for the hydrolysis of AB are listed in Table 3 for comparison.

3.4. Reusability of Co–P catalyst in the hydrolytic dehydrogenation of AB

The Co–P/TiO₂ catalyst was also tested for its isolability and reusability in the hydrolytic dehydrogenation of AB. After the complete hydrolytic dehydrogenation of 50 mM H₃NBH₃ solution catalyzed by Co–P/TiO₂ catalyst (25 mg) at 25 ± 0.5 °C, the catalyst was isolated as black powder, washed with water and methanol, and dried in the oven at 60 °C. The isolated samples of the Co–P/TiO₂ catalyst are redispersible in aqueous solution and yet active in the hydrolytic dehydrogenation of AB. Fig. 11 shows the retained percent catalytic activity of the Co–P/TiO₂ catalyst after successively repeated hydrolytic dehydrogenation, isolation and redispersion cycles at 25 ± 0.5 °C. It is noteworthy that Co–P/TiO₂ catalyst retains 92% of its initial activity even at the sixth run in the

hydrolytic dehydrogenation of AB with a complete release of hydrogen. However, the slight decrease in catalytic activity in subsequent runs may be attributed to the passivation of the catalyst surface by increasing the concentration of boron products, e.g. metaborate, which decreases the accessibility of active sites [43] or to the loss of catalyst during isolation processes after previous runs. As a result, Co–P/TiO₂ catalyst is isolable, redispersible and yet catalytically active in the hydrolytic dehydrogenation of AB.

4. Conclusions

In summary, this study on the kinetics of the hydrolytic dehydrogenation of AB using Co–P/TiO₂ catalyst has led to the following conclusions and insights: It is found that Co–P/TiO₂ is active and reusable catalyst in the hydrolytic dehydrogenation of AB even at low concentrations and temperature. Moreover, the complete release of hydrogen is achieved even in successive runs performed by dispersing the catalyst isolated after each run. When redispersed in aqueous solution of AB, Co–P/TiO₂ catalyst retains 92% of its initial activity even at the sixth run with a complete release of hydrogen. The hydrolytic dehydrogenation of AB catalyzed by Co–P/TiO₂ was found to be first order with respect to catalyst amount and zero order with respect to AB concentration. The high catalytic activity and reusability of Co–P/TiO₂ catalyst make it a promising candidate to be used as catalyst in developing highly efficient portable hydrogen generation systems using AB as solid hydrogen-storage material.

Acknowledgment

The SEM-EDX, XRD and XPS analyses were carried out at the Central Laboratory of Middle East Technical University.

References

- [1] A.J. Hung, S.F. Tsai, Y.Y. Hsu, J.R. Ku, Y.H. Chen, C.C. Yu, *Int. J. Hydrogen Energy* 33 (2008) 6205–6215.
- [2] Z. Li, G. Zhu, G. Lu, S. Qiu, X. Yao, *J. Am. Chem. Soc.* 132 (2010) 1490–1491.
- [3] S. Orimo, Y. Nakamori, J.R. Eliseo, A. Züttel, C.M. Jensen, *Chem. Rev.* 107 (2007) 4111–4132.
- [4] S. Satyapal, C. Read, G. Ordaz, G. Thomas, Annual DOE Hydrogen Program Merit Review: Hydrogen Storage, U.S. Department of Energy, Washington, DC, 2006. Available from: http://www.hydrogen.energy.gov/pdfs/review06/2_storage_satyapal.pdf.
- [5] F.H. Stephens, V. Pons, R.T. Baker, *Dalt. Trans.* 25 (2007) 2613–2626.
- [6] B. Peng, D. Chen, *Energy Environ. Sci.* 1 (2008) 479–483.
- [7] T. Umegaki, J.M. Yan, X.B. Zhang, H. Shioyama, N. Kuriyama, Q. Xu, *Int. J. Hydrogen Energy* 34 (2008) 2303–2311.
- [8] T. Umegaki, J.M. Yan, X.B. Zhang, H. Shioyama, N. Kuriyam, Q. Xu, *Int. J. Hydrogen Energy* 34 (2009) 3816–3822.
- [9] H.B. Dai, Y. Liang, P. Wang, H.M. Cheng, *J. Power Sources* 177 (2008) 17–23.
- [10] H.B. Dai, L.L. Gao, Y. Liang, X.D. Kang, P. Wang, *J. Power Sources* 195 (2010) 307–312.
- [11] T. Umegaki, T. Ohashi, Q. Xu, Y. Kojima, *Mater. Res. Bull.* 52 (2014) 117–121.
- [12] L. Yang, N. Cao, C. Du, H. Dai, K. Hu, W. Luo, G. Cheng, *Mater. Lett.* 115 (2014) 113–116.
- [13] A.K. Figen, M.B. Pişkin, B. Coşkun, V. İmamoglu, *Int. J. Hydrogen Energy* 38 (2013) 16215–16228.
- [14] N. Patel, R. Fernandes, S. Gupta, R. Edla, D.C. Kothari, A. Miotello, *Appl. Catal. B* 140–141 (2013) 125–132.
- [15] A.K. Figen, *Int. J. Hydrogen Energy* 38 (2013) 9186–9197.
- [16] T. Umegaki, C. Takei, Y. Watanuki, Q. Xu, Y. Kojima, *J. Mol. Catal. a* 371 (2013) 1–7.
- [17] A.K. Figen, B. Coşkun, *Int. J. Hydrogen Energy* 38 (2013) 2824–2835.
- [18] T. Umegaki, Q. Xu, Y. Kojima, *J. Power Sources* 216 (2012) 363–367.
- [19] M. Dinç, Ö. Metin, S. Özkar, *Catal. Today* 183 (2012) 10–16.
- [20] M. Rakap, S. Özkar, *Catal. Today* 183 (2012) 17–25.
- [21] C.H. Liu, Y.C. Wu, C.C. Chou, B.H. Chen, C.L. Hsueh, J.R. Ku, F. Tsau, *Int. J. Hydrogen Energy* 37 (2012) 2950–2959.
- [22] N. Patel, A. Kale, A. Miotello, *Appl. Catal. B* 111–112 (2012) 178–184.
- [23] N. Patel, R. Fernandes, A. Santini, A. Miotello, *Int. J. Hydrogen Energy* 37 (2012) 2007–2013.
- [24] Ö. Metin, M. Dinç, Z.S. Eren, S. Özkar, *Int. J. Hydrogen Energy* 36 (2011) 11528–11535.
- [25] V.I. Simagina, O.V. Komova, A.M. Ozerova, O.V. Netskina, G.V. Odegova, D.G. Kellerman, O.A. Bulavchenko, A.V. Ishchenko, *Appl. Catal. a* 394 (2011) 86–92.
- [26] J. Yang, F. Cheng, J. Liang, J. Chen, *Int. J. Hydrogen Energy* 36 (2011) 1411–1417.
- [27] T. Umegaki, J.M. Yan, X.B. Zhang, H. Shioyama, N. Kuriyama, Q. Xu, *J. Power Sources* 195 (2010) 8209–8214.
- [28] M. Rakap, S. Özkar, *Int. J. Hydrogen Energy* 35 (2010) 3341–3346.
- [29] N. Patel, R. Fernandes, G. Guella, A. Miotello, *Appl. Catal. B* 95 (2010) 137–143.
- [30] J.M. Yan, X.B. Zhang, H. Shioyama, Q. Xu, *J. Power Sources* 195 (2010) 1091–1094.
- [31] J.M. Yan, X.B. Zhang, S. Han, H. Shioyama, Q. Xu, *J. Power Sources* 194 (2009) 478–481.
- [32] R. Fernandes, N. Patel, A. Paris, L. Calliari, A. Miotello, *Int. J. Hydrogen Energy* 38 (2013) 3313–3322.
- [33] Y. Liang, P. Wang, H.B. Dai, *J. Alloys Compd.* 491 (2010) 359–365.
- [34] N. Malvadkar, S. Park, M.U. MacDonald, H. Wang, M.C. Demirel, *J. Power Sources* 182 (2008) 323–328.
- [35] M. Rakap, E.E. Kalu, S. Özkar, *Int. J. Hydrogen Energy* 36 (2011) 254–261.
- [36] A.S. Kuruganti, K.S. Chen, E.E. Kalu, *Electrochem. Solid-state Lett.* 2 (1999) 27–29.
- [37] D. Fox, E.E. Kalu, *Electrochem. Commun.* 9 (2007) 584–590.
- [38] K. Eom, K. Cho, H. Kwon, *Int. J. Hydrogen Energy* 35 (2010) 181–186.
- [39] A.B. Mandale, S. Badrinarayanan, S.K. Date, A.P.B. Sinha, *J. Electron Spectrosc. Relat. Phenom.* 33 (1984) 61–72.
- [40] L. Gucci, D. Bazin, *Appl. Catal. a* 188 (1999) 163–174.
- [41] N.S. McIntyre, M.G. Cook, *Anal. Chem.* 47 (1975) 2208–2213.
- [42] P.V. Ramachandran, P.D. Gagare, *Inorg. Chem.* 46 (2007) 7810–7817.
- [43] C.A. Jaska, T.J. Clark, S.B. Clendenning, D. Groeza, A. Turak, Z.H. Lu, I. Manners, *J. Am. Chem. Soc.* 127 (2005) 5116–5124.
- [44] Y.C. Luo, Y.H. Liu, Y. Hung, X.Y. Liu, C.Y. Mou, *Int. J. Hydrogen Energy* 38 (2013) 7280–7290.
- [45] O. Akdim, U.B. Demirci, P. Miele, *Int. J. Hydrogen Energy* 38 (2013) 5627–5637.
- [46] M. Rakap, E.E. Kalu, S. Özkar, *J. Power Sources* 210 (2012) 184–190.
- [47] Q. Xu, M. Chandra, *J. Power Sources* 163 (2006) 364–370.
- [48] O. Ozay, E. Inger, N. Aktaş, N. Şahiner, *Int. J. Hydrogen Energy* 36 (2011) 8209–8216.
- [49] P. Song, Y. Li, W. Li, B. He, J. Yang, X. Li, *Int. J. Hydrogen Energy* 36 (2011) 10468–10473.